Available online at www.sciencedirect.com
SCIENCE DIRECT®
International Journal of Heat and Mass Transfer 47 (2004) 4277–4284
International Journal of HEAT and MASS TRANSFER
www.elsevier.com/locate/ijhmt

Effect of liquid layering at the liquid–solid interface on thermal transport

L. Xue [a], P. Keblinski [a,*], S.R. Phillpot [b,c], S.U.-S. Choi [d], J.A. Eastman [b]

[a] Department of Materials Science and Engineering, Rensselaer Polytechnic Institute, Troy, NY 12180-3590, USA
[b] Materials Science Division, Argonne National Laboratory, Argonne, IL 60439, USA
[c] Department of Materials Science and Engineering, University of Florida, Gainesville, FL 32611-6400, USA
[d] Energy Technology Division, Argonne National Laboratory, Argonne, IL 60439, USA

Received 30 October 2003; received in revised form 29 April 2004

Abstract

Using non-equilibrium molecular dynamics simulations in which a temperature gradient is imposed, we study how the ordering of the liquid at the liquid–solid interface affects the interfacial thermal resistance. Our simulations of a simple monoatomic liquid show no effect on the thermal transport either normal to the surface or parallel to the surface. Even for of a liquid that is highly confined between two solids, we find no effect on thermal conductivity. This contrasts with well-known significant effect of confinement on the viscoelastic response. Our findings suggest that the experimentally observed large enhancement of thermal conductivity in suspensions of solid nanosized particles (nanofluids) can not be explained by altered thermal transport properties of the layered liquid.

Keywords: Interfacial thermal resistance; Liquid–solid interface; Molecular dynamics simulations; Nanofluids

1. Introduction

A liquid in contact with a solid interface is significantly more ordered than a bulk liquid. In the direction normal to the liquid–solid interface, liquid density profiles exhibit oscillatory behavior on the molecular scale due to interactions between the atoms in the liquid and the solid [1,2]. The magnitude of the layering increases with increasing solid–liquid bonding strength, and the layering extends into the liquid over several atomic or molecular distances. In addition, with increasing strength of the liquid–solid bonding, crystal-like order develops in the liquid in the lateral directions. These structural changes have pronounced effects on a number of properties, including the liquid–solid phase transition [3–5], flow and tribological properties [6–9]. The nature of the solid–liquid molecular interactions and the surface topology also play a critical role in determining the mechanical properties of confined liquid films. In particular, the degree by which the viscosity is increased due to confinement and solidification is still a topic of intense discussion [10]. Liquid layering also leads to oscillatory forces between macroscopic bodies separated by a liquid layer of several atomic distances [11].

Given that ordering of the liquid at the solid–liquid interface has a major effect on mechanical properties, it is important to address the issue of the effects of liquid ordering on thermal transport properties. One indication that such ordering could be important comes from the elementary observation that the thermal conductivity of completely ordered crystalline materials is typically much larger than that of disordered amorphous materials. The efficient thermal transport in solids arises from lattice vibrations (phonons) that are able to move ballistically over relatively large distances (the phonon

* Corresponding author. Tel.: +1-518-276-6858; fax: +1-518-276-8554.
E-mail address: keblip@rpi.edu (P. Keblinski).

0017-9310/$ - see front matter © 2004 Elsevier Ltd. All rights reserved.
doi:10.1016/j.ijheatmasstransfer.2004.05.016

mean free path) before being scattered either from other lattice excitations or from structural defects in the crystal. By contrast the absence of order in liquids (and amorphous materials) eliminates this effective heat transport mechanism, resulting in an effective mean free path being only of the order of an atom size. If the ordering in the liquid is capable of increasing the distance over which the heat wave moves in a ballistic manner, it should have a significant effect on the thermal transport properties in the interface region.

By contrast to a possible enhancement of the conductivity of the interfacial liquid, the mismatch between properties of liquid and solid generally leads to a thermal resistance, known since the pioneering work on the metal–liquid helium interface by Kapitza [12]. Due to the relatively good contact between liquid and solid, this interfacial resistance, also known as the Kapitza resistance, is rather low. From the macroscopic point of view the net interfacial resistance will express the balance between discontinuity-related resistance and possible thermal conductivity enhancement due to liquid ordering.

The current theoretical understanding of the thermal resistance of solid–liquid interfaces is primarily based on the "acoustic mismatch model" (AMM) in which one considers the transmission and reflection of classical heat waves at the interface [13]. However, the AMM, derived from the requirements of continuity at the interfaces, includes only the bulk properties of the two materials, with no account being taken of the nature of the bonding between liquid and solid atoms at the interface, or of the ordering of the liquid structure at the interface. In fact, the results of our recent molecular dynamics (MD) simulations revealed that the strength of the bonding between liquid and solid atoms plays a key role in determining the temperature drop at the solid–liquid interface [14]. Similar conclusions were obtained by Maruyama and Kimura [15], and Barrat and Chiaruttini [16], who drawn an analogy between the Kapitza resistance and hydrodynamic slip length.

In addition to its intrinsic scientific interest, understanding the solid–liquid interface thermal resistance is now becoming a technological imperative also, driven by the measured significant enhancements in the thermal-transport properties of nanofluids, i.e., suspensions of solid nanoparticles in liquids [17]. For example, experiments have shown that for Cu–water nanofluids, a mere 0.3 vol% of ~10 nm Cu nanoparticles leads to an up to 40% increase of thermal conductivity, more than an order of magnitude above the increase predicted by macroscopic theory [18]. Because interfaces are expected to provide resistance to the heat flow [19], their prevalence in nanofluids should actually be detrimental to the overall thermal conductivity. Indeed, our previous molecular dynamics simulations [14] demonstrated that even in the case of the strongly wetting solid there is a temperature drop at the solid–liquid interface, associated with the Kapitza resistance. The Kapitza resistance becomes even more pronounced for weakly or non-wetting interfaces [14–16]. Ordering of the liquid layers is one possible mechanism to counterbalance this resistance. Despite the fact that the ordered liquid is only several atomic distances thick, a substantial volume fraction of the liquid is within a few atomic distances from the solid, and thus the properties of the ordered liquid layers could have a significant impact on thermal transport in nanofluids.

Based on the assumption that the layered liquid has significantly larger thermal conductivity than a non-layered liquid, it has been demonstrated that a continuum-level model is capable of predicting the thermal conductivity enhancement in Al_2O_3 nanoparticle/water and carbon nanotube/oil nanofluids [20]. However, for the model to agree with experiment, it was necessary to assume both that the conductivity of the structured liquid is several times larger than that of the bulk liquid, and that liquid layer is of the order of 3 nm thick. While the first assumption is questionable, the second assumption is known to be incorrect for simple liquids: both experiment and simulation show significant ordering extends only to a few atomic distances, i.e., ~1 nm. It is, however, possible that more complex liquids have ordering effects extending over longer distances from the interfaces. For example, if nanoparticles are charged, an associated electric field might induce longer range ordering in polar liquids.

The objective of this paper is to use MD simulations to identify the relationship between the liquid structure at the solid interface and its thermal transport characteristics. Due to the detailed information on atomic level structure and dynamics that it can provide, molecular dynamics (MD) simulation is ideally suited for this task, and in recent years has increasingly been used to study various thermal transport problems, including interfacial related problems [21]. In this first study of its kind we will limit ourselves to simulations of simple liquids comprise of monoatomic "molecules". For this model system we find that, in contrast to the significant effects on mechanical properties discussed above, the liquid layering actually has a surprisingly small effect on the thermal transport characteristics. Indeed, both in the directions normal and parallel to the solid–liquid interface, we find that the thermal conductivity of the layered liquid is indistinguishable from that of the bulk liquid, both for solid–liquid interaction parameters corresponding to wetting and non-wetting situations. By contrast, the Kapitza resistance is a strong function of wetting properties [14–16]. For a wetting liquid, the strong bonding between solid and liquid atoms, means that energy transport is quite efficient at the boundary; i.e., the Kapitza resistance is low. Similarly, the weak solid–liquid bonding for a non-wetting liquid results in

poor energy transport across the interface, and a high Kaptiza resistance. We discuss the origin of the surprisingly small effects of liquid ordering and potential implications for our understanding of heat flow at solid–liquid interfaces.

2. Simulation model and method

Because our work represent the first detailed analysis of the role of liquid ordering on thermal transport, rather than modeling specific materials, we use a simple atomic liquid with interactions described by the Lennard-Jones (LJ) interatomic potential, whose properties [22], including thermal-transport properties [23], have been thoroughly characterized in numerous simulations. As in our recent simulations of the thermal resistance at a solid–liquid interface [14], and for simplicity, the interactions between solid atoms, liquid atoms, and solid–liquid atoms are all described by the LJ potential. Within such a model the pair interaction potential is given by

$$U_{\alpha\beta}(r_{ij}) = \varepsilon_{\alpha\beta}\left[\left(\frac{\sigma_{\alpha\beta}}{r_{ij}}\right)^{12} - \left(\frac{\sigma_{\alpha\beta}}{r_{ij}}\right)^{6}\right], \tag{1}$$

where r_{ij} is the interatomic spacing between atoms i and j, α and β refer to liquid (l) or solid (s) species and ε and σ are parameters describing the bonding energy and bonding distance respectively. In our model we will use the liquid parameters to set up the length scale, $\sigma_{ll} \equiv \sigma$ and the energy scale, $\varepsilon_{ll} \equiv \varepsilon$. We will follow the custom of reporting results for simulations of LJ materials in so-called reduced units, which allow simulations with different values of σ and ε to be compared directly. All simulations are performed at the reduced temperature of $T^* = k_B T/\varepsilon = 0.70$, and the liquid reduced density, $\rho^* = \rho/\sigma^3 = 0.84$. This temperature and density are close to the triple point of the LJ potential; such or similar conditions are typically used in molecular simulations of thermal transport [23,15,24] and represent a generic liquid near its triple point.

Because the melting point for the LJ potential is proportional to ε, the value of ε_{ss} must be significantly larger than ε_{ll}; we have made the somewhat arbitrary choice $\varepsilon_{ss} = 10\varepsilon_{ll}$. This mimics a "generic" solid with a face centered cubic (fcc) crystalline structure, which is well bellow its melting point. Due to stability of such defined solid, we do not need to introduce any additional spring holding the solid atoms at the crystalline sites [15,24] thus we naturally capture the dynamics of the phonons in the solid phase [14].

For simplicity, and in the spirit of this being a simulation of a generic system, the mass of the solid atoms is taken to be the same as the mass of the liquid atoms and all $\sigma_{\alpha\beta}$ are taken to have the same value (i.e., the solid and liquid atoms have the same size). This leads to the density of the solid being just 20% larger than the density of the liquid due to better packing; for real materials the density of the solid is typically several times larger than that of the liquid. Interestingly the very small number density mismatch can be expected to enhance the effect of ordering in the liquid on the thermal conductivity relative to that of real solid–liquid systems; thus from this perspective we would expect our simulations to tend to overestimate any enhancement. Nevertheless, from the point of view of interfacial thermal resistance, the relevant macroscopic parameter is the mismatch between the acoustic impedances of the two media, $Z = \rho c$, where ρ is the density and c is the speed of sound [13]. Considering that the speed of sound is proportional to $\sqrt{E/\rho}$, where E is elastic modulus, and that E is proportional to the energy bonding parameter (ε), one gets the ratio of $Z_{solid}/Z_{liquid} \sim \sqrt{\varepsilon_{ss}\rho_s/\varepsilon_{ll}\rho_l} \approx 4$ for our model. Thus our model captures the acoustic mismatch characteristic of solid–liquid interfaces.

In our previous studies we determined the Kapitza resistance of a similar model system as a function of the solid–liquid interactions strength [14]. In particular we observed two different regimes of the Kapitza resistance dependence on ε_{ls}, with a dividing value $\varepsilon_{ls} \approx \varepsilon$. For this study we select two values of the solid–liquid bonding energy parameter, ε_{ls}. The first choice, $\varepsilon_{ls} = \sqrt{10}\varepsilon \approx 3.3\varepsilon$ corresponds to a wetting liquid [25], for which the bonds between solid and liquid atoms are stronger than those among liquid atoms; this also corresponds to the traditional form for the interaction potentials of $\varepsilon_{ls} = \sqrt{\varepsilon_{ss}\varepsilon_{ll}}$ [22]. For the simulations of a non-wetting liquid, in which the bonds among the liquid atoms are stronger than those between solid and liquid, we chose $\varepsilon_{ls} = 0.2\varepsilon$. These two choices will allow us to expose differences between two main classes of the solid–liquid interfaces and the effects of the degree of liquid structuring which, due to the strong solid–liquid interactions, is much more pronounced for wetting liquids.

The total force acting on each atom is computed as the sum of the pair-wise forces originating from the LJ potential (Eq. (1)). For computational efficiency, we use a cutoff for the interatomic potential of 2.3σ, which is in a typical range used in simulations of LJ systems, and has been demonstrated to be sufficiently large for thermal transport calculations [23]; to avoid discontinuities in the integration of the numerical equations of motion, we follow the customary procedure of shifting the forces and energies such that they are zero at the cutoff. The Newton's equation of motion, $F = ma$, where m is the mass of an atom, F is the net force acting on an atom and a is acceleration are solved using fifth order predictor–corrector integrator [22]. We use an MD time step of $0.001\tau^*$, where $\tau^* = [\varepsilon/m\sigma^2]^{1/2}$, which conserves energy in microcanonical–ensemble simulations to four significant figures over one million MD steps [26]. This

ensures very good energy conservation over the entire length of the simulation run.

The geometry of the simulation cell is depicted in Fig. 1. Initially, it consists of a square cylinder of [1 0 0]-oriented perfect fcc crystal of length $80a_0$ in the z-direction and width $7a_0$ in the x- and y-directions, where $a_0 = 1.56\sigma$ is the cubic lattice parameter. The simulation cell thus contains a total of $80\times7\times7\times4 = 15{,}680$ atoms. To mimic a system of infinite extent without any surfaces, periodic boundary conditions are applied in all three directions. We divide the simulation cell along the z-direction into eight slabs of alternating solid and liquid. All of the solid slabs are $10a_0$ wide; for reasons discussed below, in most of our simulations two of the liquid-atom designated slabs are initially $18a_0$ wide while the other two are $2a_0$ wide. This structure is first heated at constant volume and the reduced temperature $T^* = 1.40$ which leads to melting of the liquid slabs; it then is equilibrated at the $T^* = 0.70$. During this equilibration the size of the simulation cell is allow to change according to the constant pressure algorithm [22], such that pressure is the same as for the bulk liquid at $T^* = 0.70$ and $\rho^* = 0.84$, i.e., close to the triple point of the LJ potential [23]. By ensuring equal hydrostatic pressures in the liquid slabs in the two cases, we can make a meaningful comparison of the results between wetting and non-wetting cases.

Following equilibration, we apply a heat source and a heat sink in the middle of two narrow liquid regions, as shown in Fig. 1, by rescaling velocities such that the heat is added at the source at constant rate $\mathrm{d}Q/\mathrm{d}t$ and removed at the same rate at the sink; the energy of the system is thus conserved. This velocity rescaling procedure is augmented with a correction ensuring momentum conservation [27]. With the above choice of simulation-cell geometry, the system contains eight liquid–solid interfaces, four of them well separated from the heat source and sink and adjacent to wide liquid slabs. This allows us to minimize possible spurious effects associated with the heat sources, and to compare the properties of the structured liquid at the interface with bulk liquid sufficiently away from the interface.

Prior to taking averages we simulate for 500,000 MD steps such that the system reaches a steady state, with a constant flux of $\mathrm{d}Q/\mathrm{d}t/A$, where A is the cross-sectional area. To monitor the temperature the simulation cell is divided into 160 virtual slices along the thermal flux (z)-direction and the temperature profiles (separate for liquid and solid) are then obtained by time averaging the temperature of each slice over 2,000,000 MD simulation steps. We verified that after initial 500,000 MD steps, the temperature profiles obtained by time averaging over subsequent 500,000 MD steps time windows are identical (within the expected thermodynamic fluctuations); this is a signature of a steady state. During simulations we also collect data on the atomic configurations and the density profiles of both liquid and solid.

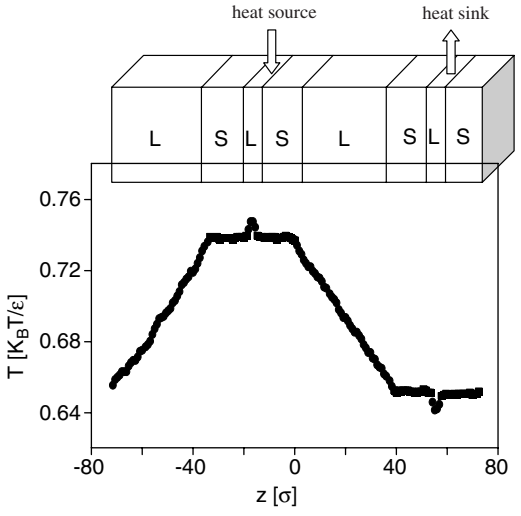

Fig. 1. Top panel: schematic of the model system containing four solid slabs separated by four liquid slabs; the regions where heat is added and removed from the system are indicated by arrows. Bottom panel: a typical temperature profile showing a smooth temperature decrease through the liquid, an essentially constant temperature in the solid.

3. Results

The bottom panel in Fig. 1 shows the temperature profiles obtained for the wetting case using the simulation procedure described above. Due to the periodic boundary conditions, the temperature vs. position curve is symmetric about both the heat source and heat sink. As clearly seen in Fig. 1, there are large temperature gradients in all of the liquid regions and almost flat temperature profiles in the solid regions; these correspond to low thermal conductivity and very high thermal conductivity respectively. In fact, the almost flat temperature profiles in the solid slabs are also associated with the fact that the solid slab thickness is smaller than the phonon mean free path, leading to ballistic thermal energy transport across the solid regions [17]. In the case of the wetting liquid depicted in Fig. 1, the actual temperature drop at the solid–liquid interface is relatively small and thus not visible on the scale of the figure; however, examination of the data itself shows that, consistent with our earlier study [14], there is indeed such a drop.

To explicitly show the layering of the liquid at the solid–liquid interface, we plot the x–z projection of the atomic configuration at a solid–liquid interface for the wetting (top) and non-wetting (bottom) cases in Fig. 2. From Fig. 2 we can see that for the wetting liquid,

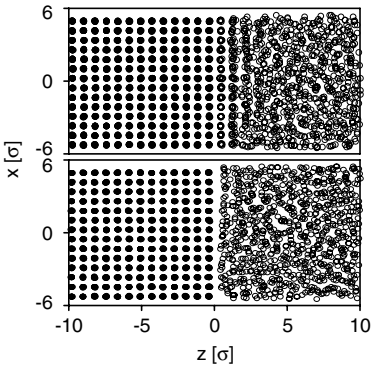

Fig. 2. Atomic configuration (x–z plane projection) at a solid liquid interface for the wetting and non-wetting liquids. The interface is at $z = 0$ and the liquid is at the right side.

because of the strong interaction between the liquid and solid atoms, the liquid exhibits strong ordering over a distance of several atomic sizes (up to $\sim 4\sigma$). By contrast for the non-wetting case the layering is very weak, and is essentially limited to a single layer of liquid atoms.

Fig. 3 shows the cross sectional configuration (x–y projection) of the first liquid layer near the wetting solid–liquid interface. We can clearly see that the liquid atoms are in a perfect (1 0 0) fcc plane configuration patterned after the fcc structure of the neighboring solid. To quantify the degree and the extent of crystallinity in the plane we monitor the square of the planar structure factor, $S(k)$, which we denote by $S^2(k)$ [28]:

$$|S(k)|^2 = S^2(k) = \left[\frac{1}{N}\sum_{i=1}^{N}(\cos k \cdot r_i)\right]^2 + \left[\frac{1}{N}\sum_{i=1}^{N}(\sin k \cdot r_i)\right]^2 \quad (2)$$

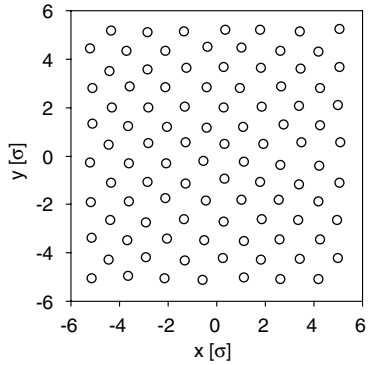

Fig. 3. Cross sectional atomic configuration (x–y plane projection) of the first liquid layer near the solid–liquid interface for the wetting liquid.

where r_i is the position of atom i in a given plane (x_i, y_i) and N is the number of atoms in this plane. At $T = 0$ K in the perfect crystal structure, $S^2(k)$ is then unity for any wave vector k that is a reciprocal lattice vector of the plane. By contrast, in the liquid or amorphous states, $S^2(k)$ fluctuates near zero due to the absence of long range order. Thus $S^2(k)$ provides us a measure of the degree of crystallinity of every lattice plane.

The structure factor profiles at the vicinity of the solid–liquid interface for wetting and non-wetting liquid are shown in Fig. 4. For the non-wetting case, the structure factor drops quickly from nearly unity to zero at the solid–liquid interface. But for the strong wetting case, the structure factor drops more slowly, over a distance of several atomic sizes. We thus conclude that the wetting liquid exhibits strong ordering in both normal and parallel directions over a distance of several atomic sizes, whereas for the non-wetting liquid, the ordering is weak.

To analyze the effect of this layering on the thermal transport properties, in Fig. 5 we present the averaged

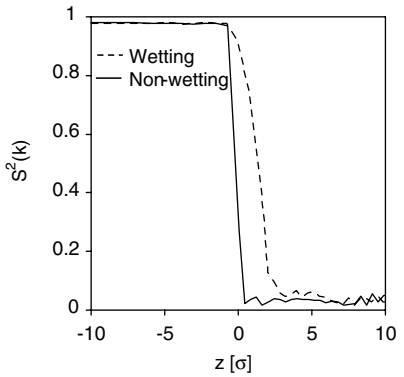

Fig. 4. Structure factor profiles at the vicinity of the solid–liquid interface for the wetting and non-wetting liquids. The interface is at $z = 0$ and the liquid is at the right side.

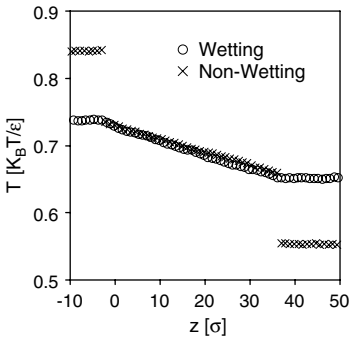

Fig. 5. Temperature profiles for the sandwiched liquid region with part of its neighboring solid regions for the wetting and non-wetting liquids.

temperature profiles over the two wide liquid regions that are far away from the heat source and heat sink (see Fig. 1). The data show a strong dependence of the temperature drop at the interface on the strength of the solid – liquid interactions, as discussed in detail in Ref. [14], with a relatively small drop for the wetting liquid and a very large drop for the non-wetting liquid. However, the slopes of the temperature vs. position plots for the two cases are nearly the same all the way from the interface, where the liquid is structured, to the middle of the liquid region, where the molecular structure of the liquid is indistinguishable from the bulk liquid. These data indicate that the layering and ordering in the interfacial liquid has little or no effect on its thermal transport properties.

In order to show this more clearly, in Fig. 6 we also plot the density profiles along with the temperature profiles at the vicinity of the solid–liquid interface for wetting and non-wetting liquids. Consistent with the data presented in Figs. 2 and 4, for the wetting case (Fig. 6(a)) the liquid density profile exhibits oscillations due to liquid layering that persist over several atomic distances from the solid surface. By contrast, for the non-wetting case (Fig. 6(b)), there is essentially no signature of layering in the liquid. However, the slopes in the temperature profiles are the same for both cases, despite very different degrees of ordering. This reinforces our main conclusion that the liquid ordering has negligible effect on its thermal transport characteristics.

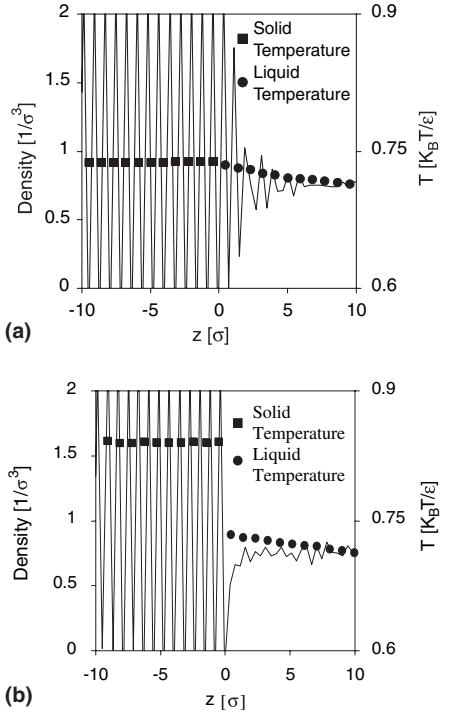

Fig. 6. (a) Distributions of number density of atoms (solid line) and average temperatures of the atomic layers (dots) at the liquid–solid interface for the wetting liquid. (b) Same as in (a) but for the non-wetting liquid. In both figures the interface is at $z = 0$.

To further assess the role of structuring, we considered a wetting liquid, in which the width of the liquid layer is reduced to 3.6σ. Although for the 3.6σ width layer, the liquid is highly confined and ordered and involves only 4 layers of liquid atoms, Fig. 7 shows that there is no difference between the temperature gradients in the two systems. This shows that even when the whole liquid region is ordered, there is still no significant effect on the thermal transport properties.

Finally we address the effect of liquid ordering on lateral thermal transport. In this case we prepare a structure with initial dimensions of $9a_0 \times 7a_0 \times 40a_0$ containing one solid slab elongated in the z-direction with dimensions of $2a_0 \times 7a_0 \times 40a_0$, adjacent to a slab of liquid with initial dimensions of $7a_0 \times 7a_0 \times 40a_0$. In this simulation we keep the solid atoms at their fixed perfect crystal positions, as to study only heat flow along the liquid region (see Fig. 8, top panel). We first equilibrate the wetting liquid in the presence of solid at $k_B T/\varepsilon_{ll} = 0.70$ and adjust the size of the simulation cell, such that the pressure in the liquid is the same as in our previous simulations. Then we apply the heat source and heat sink to the liquid atoms in the manner described in Sect. II. The rate of heat addition and removal is such that the thermal flux, $dQ/dt/A$, is the same as the simulations with the previous geometry.

The bottom panel in Fig. 8 shows the temperature profiles in a liquid layer sandwiched between two solid interfaces with the heat flux direction parallel and normal to the solid–liquid interface. We see that the temperature profiles are essentially the same as in the case of the heat flux normal to the interface, indicating that, as in the case of out-of-plane layering, the in-plane struc-

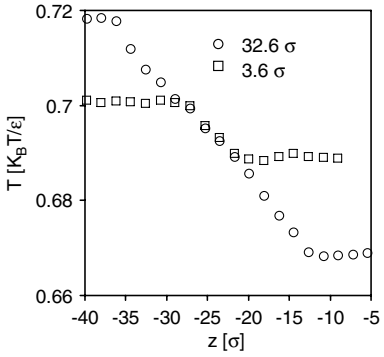

Fig. 7. Temperature profiles for the liquid region with part of its neighboring solid regions for the liquid layer thickness equals to 32.6σ and 3.6σ, respectively.

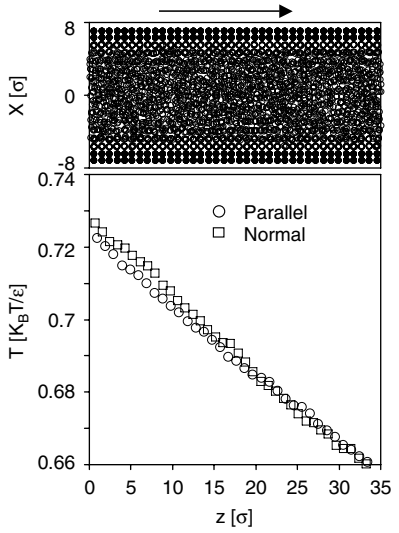

Fig. 8. Top panel: atomic structure of the liquid (open symbols) sandwiched between two solid interfaces with a frozen crystal structure. The arrow indicates the direction of the heat flux. Bottom panel: temperature profiles in liquids sandwiched between two solid interfaces with the heat flux direction parallel (top panel) and normal (Fig. 1) to the solid–liquid interfaces.

tural ordering in the liquid has no effect on the in-plane thermal transport.

4. Summary and discussion

In summary, using molecular dynamics simulations and simple liquid–solid interfaces we have demonstrated that the layering of the liquid atoms at the liquid–solid interface does not have any significant effect on thermal transport properties. These results show that one of the proposed mechanisms for the observed enhancement in the thermal transport of nanofluids is not viable. However, we cannot exclude the possibility that more complex liquids, such as those involving larger, chain-like molecules might show different relationship between the ordering and thermal transport properties.

We can speculate on the origin of the lack of any effect of structural ordering on thermal transport properties in a simple liquid. One possible explanation is that despite the large degree of ordering these liquid layers are still more disordered than the crystal; furthermore, the width of the significantly ordered region is at most several atomic distances. In such a case it is known that even for crystalline structures, finite size effects greatly reduce thermal conductivity. Moreover, the solid surface might act as a scattering site for collective motion of atoms that might otherwise developed in an ordered liquid. However, the fact that the simulations demonstrate, within the statistical accuracy, no ordering effects on thermal transport is quite intriguing, particularly in the view of other properties, most notably, liquid mobility and viscosity, being strongly altered.

We need to emphasize that our results are obtained for the specific model system involving a simple (monoatomic) liquid. More complex liquids, such as water or liquids of molecular chains, might behave differently. It is interesting to note that many metals (in the molten state they can be considered as simple liquids) exhibit no visible discontinuity in the thermal transport coefficient upon melting [29]. Thus it appears that in such systems the crystalline order at the melting point is insufficient to affect thermal conductivity; however, a significant contribution to the heat transport in crystalline and molten metals is due to electrons and not phonons. By contrast the thermal conductivity of liquid water is $\sim$4 times smaller than that of ice at the melting point [30]. In future studies we will address the role of the ordering on thermal transport of more complex liquids.

Acknowledgements

This work was supported by US Department of Energy, Office of Basic Energy Sciences, Division of Materials Sciences and Engineering, under Contract no. W-31-109-Eng-38. LX and PK were also supported by the Petroleum Research Fund, Grant no. PRF 36305-G9, and by DOE Grant no. DE-FG02-04ER46104.

References

[1] J.R. Henderson, F. Van Swol, On the interface between a fluid and a planar wall: theory and simulations of a hard sphere fluid at a hard wall, Mol. Phys. 51 (1984) 991–1010.
[2] C.-J. Yu, A.G. Richter, A. Datta, M.K. Durbin, P. Dutta, Molecular layering in a liquid on a solid substrate: an X-ray reflectivity study, Physica B 283 (2000) 27–31.
[3] P.A. Thompson, G.S. Grest, M.O. Robbins, Phase transitions and universal dynamics in confined films, Phys. Rev. Lett. 68 (1992) 3448–3451.
[4] J. Klein, E. Kumacheva, Confinement-induced phase transition in simple liquids, Science 269 (1995) 816–819.
[5] A.L. Demirel, S. Granick, Glasslike transition of a confined simple fluid, Phys. Rev. Lett 77 (1996) 2261–2264.
[6] P.A. Thompson, M.O. Robbins, Shear flow near solids: epitaxial order and flow boundary conditions, Phys. Rev. A 41 (1990) 6830–6837.
[7] B. Bhushan, J.N. Israelachvili, U. Landman, Nanotribology: friction, wear and lubrication at the atomic scale, Nature 374 (1995) 607–616.
[8] S.T. Cui, P.T. Cummings, H.D. Cochran, Molecular dynamics simulation of the rheological and dynamical properties of a model alkane fluid under confinement, J. Chem. Phys. 111 (1999) 1273–1280.
[9] J.P. Gao, W.D. Luedtke, U. Landman, Structures, solvation forces and shear of molecular films in a rough nanoconfinement, Tribol. Lett. 9 (2000) 3–13.

[10] Y. Zhu, S. Granick, Reassessment of solidification in fluids confined between mica sheets, Langmuir 19 (2003) 8148–8151.
[11] J.N. Israelachvili, Intermolecular and Surface Forces, Academic, New York, 1985.
[12] P.L. Kapitza, Zh. Eksp. Theor. Fiz. 11 (1941) 1 (J. Phys. USSR 4 (1941) 181).
[13] E.T. Schwartz, R.O. Pohl, Thermal boundary resistance, Rev. Mod. Phys. 61 (1989) 605–689.
[14] L. Xue, P. Keblinski, S.R. Phillpot, S.U.S. Choi, J.A. Eastman, Two regimes of thermal resistance at a liquid–solid interface, J. Chem. Phys. 118 (2003) 337–339.
[15] S. Maruyama, T. Kimura, A study of thermal resistance over a solid–liquid interface by molecular dynamic simulations, Ther. Sci. Eng. 7 (1999) 63–68.
[16] J.-L. Barratyand, F. Chiaruttini, Kapitza resistance at the liquid solid interface, Mol. Phys. 101 (2003) 1605–1610.
[17] P. Keblinski, S.R. Phillpot, S.U.S. Choi, J.A. Eastman, Mechanisms of heat flow in suspensions of nano-sized particles (nanofluids), Int. J. Heat Mass Transfer 45 (2002) 855–863.
[18] J.A. Eastman, S.U.S. Choi, S. Li, W. Yu, L.J. Thompson, Anomalously increased effective thermal conductivity of ethylene glycol-based nanofluids containing copper nanoparticles, Appl. Phys. Lett. 78 (2001) 718–720.
[19] O.M. Wilson, X. Hu, D.G. Cahill, P.V. Braun, Colloidal metal particles as probes of nanoscale thermal transport in fluids, Phys. Rev. B 66 (2002) 224301-1–224301-6.
[20] Q.Z. Xue, Model for effective thermal conductivity of nanofluids, Phys. Lett. A. 307 (2003) 313–317.
[21] D. Poulikakos, S. Arcidiacono, S. Maruyama, Molecular dynamics simulations in nanoscale heat transfer: a review, Micro. Thermophys. Eng. 7 (2003) 181–206.
[22] M.P. Allen, D.J. Tildesley, Computer Simulation of Liquids, Oxford University Press, Oxford, 1987.
[23] R. Vogelsang, C. Hoheisel, G. Ciccotti, Thermal conductivity of the Lennard-Jones liquid by molecular dynamics calculations, J. Chem. Phys. 86 (1987) 6371–6375.
[24] T. Ohara, D. Suzuki, Intermolecular energy transfer at a solid–liquid interface, Micro. Thermophys. Eng. 4 (2000) 189–196.
[25] S. Maruyama, T. Kurashige, S. Matsumoto, Y. Yamaguchi, T. Kimura, Liquid droplet in contact with a solid surface, Micro. Thermophys. Eng. 2 (1998) 49–62.
[26] See p. 98 in Ref. [22].
[27] P. Jund, R. Jullien, Molecular-dynamics calculation of the thermal conductivity of vitreous silica, Phys. Rev. B 59 (1999) 13707–13711.
[28] S.R. Phillpot, J.F. Lutsko, D. Wolf, S. Yip, Molecular-dynamics study of lattice-defect-nucleated melting in silicon, Phys. Rev. B 40 (1989) 2831–2840.
[29] D.R. Poirier, G.H. Geiger, Transport Phenomena in Materials Processing, TMS, 1994, p. 197.
[30] D.R. Lide, CRC Handbook of Chemistry and Physics, 84th ed., CRC Press, Florida, 2003.